

Instrumental vetoes for transient gravitational-wave triggers using noise-coupling models: The bilinear-coupling veto

Parameswaran Ajith,^{1,2,3} Tomoki Isogai,^{4,5} Nelson Christensen,⁵ Rana X. Adhikari,²
Aaron B. Pearlman,^{2,6} Alex Wein,² Alan J. Weinstein,² and Ben Yuan²

¹*International Centre for Theoretical Sciences, Tata Institute of Fundamental Research, Bangalore 560012, India.*

²*LIGO Laboratory, California Institute of Technology, Pasadena, CA 91125, USA*

³*Theoretical Astrophysics, California Institute of Technology, Pasadena, CA 91125, USA*

⁴*LIGO Laboratory, Massachusetts Institute of Technology, Cambridge, MA 02139 USA*

⁵*Physics and Astronomy, Carleton College, Northfield, MN 55057, USA*

⁶*Department of Applied Physics, California Institute of Technology, Pasadena, CA 91125, USA*

LIGO and Virgo recently completed searches for gravitational waves at their initial target sensitivities, and soon Advanced LIGO and Advanced Virgo will commence observations with even better capabilities. In the search for short duration signals, such as coalescing compact binary inspirals or “burst” events, noise transients can be problematic. Interferometric gravitational-wave detectors are highly complex instruments, and, based on the experience from the past, the data often contain a large number of noise transients that are not easily distinguishable from possible gravitational-wave signals. In order to perform a sensitive search for short-duration gravitational-wave signals it is important to identify these noise artifacts, and to “veto” them. Here we describe such a veto, the bilinear-coupling veto, that makes use of an empirical model of the coupling of instrumental noise to the output strain channel of the interferometric gravitational-wave detector. In this method, we check whether the data from the output strain channel at the time of an apparent signal is consistent with the data from a bilinear combination of auxiliary channels. We discuss the results of the application of this veto on recent LIGO data, and its possible utility when used with data from Advanced LIGO and Advanced Virgo.

I. INTRODUCTION

The LIGO and Virgo laser interferometric gravitational-wave (GW) detectors recently completed their observations in their initial design configurations. While GWs were not observed, important upper limits have been established in searching for signals from coalescing compact (neutron star and black hole) binaries [1, 2], burst events [3] (core collapse supernova [4], cosmic strings [5], etc.), rapidly spinning neutron stars [6], and a stochastic GW background [7]. Searches were also made for GW signals in association with gamma ray bursts [8] and high energy neutrinos [9]. By 2015 Advanced LIGO [10] will begin operating with a significant improvement in sensitivity, followed soon thereafter by Advanced Virgo [11, 12] coming on-line in 2016-2017 [13]. A world-wide network of advanced interferometric GW detectors will be operating in the near future; a Japanese detector, KAGRA [14], is currently under construction, and a third LIGO detector may also be constructed in India.

Interferometric GW detectors are highly complex instruments; the data to date have often contained a large number of noise transients or noise frequency lines that were not easily distinguishable from possible GW signals. Noise artifacts can be created from imperfections or events within the detector itself, or caused by disturbances in the physical environment around where the detectors are located, which can couple to the output strain channel (the “GW channel”) through various coupling mechanisms. In order to perform a sensitive search for GW signals, it is important to identify these noise artifacts, and to “veto” them. For the initial LIGO and Virgo detectors, numerous techniques were developed in order to identify and remove data from time periods when problems with the detector or its physical environment could be detected [15, 16]. Similarly, specific noise frequency lines were also identified and removed from searches for GW signals from rapidly spinning

neutron stars and the stochastic GW background [17].

Short duration noise transients, or *glitches*, are especially problematic for compact coalescing binary and burst GW signal searches. During the recent LIGO (S6) and Virgo (VSR2, VSR3) scientific runs a number of vetoes were defined in order to identify and remove glitches from the interferometers’ output strain GW channel, H . During these recent scientific runs data from numerous interferometer auxiliary channels and physical environment monitoring (PEM) devices were recorded, and searched for glitches. The glitch search tool used was a wavelet-based program called *KleineWelle* (KW) [18]. The various vetoes were developed by looking for statistical association between glitches in the interferometer auxiliary channels and the PEM devices and events in the interferometer’s output strain channel. For example, the hierarchical (“hveto”) pipeline [19] and the “used percentage veto” [20] were effective in identifying noise events in the GW channel due to glitches that appeared in multiple channels in LIGO and Virgo data, while the “SeisVeto” [21] was effective in eliminating glitches that originated due to fluctuations in the seismic noise. Another veto compared KW triggers from the two quadrature phases of Virgo’s output strain channel, and when associations could be made between events in the in-phase and quadrature channels, then the in-phase events were vetoed [22]¹.

The “traditional” veto methods mentioned above all search for a time coincidence between a glitch in an interferometer’s output strain channel, and an event in an interferometer auxiliary or PEM channel. The *bilinear-coupling veto*, which we are describing in this paper, was developed with the goal to see if the data from an interferometer’s output GW strain channel at the time of an apparent signal is consistent with the data

¹ Another veto method making use of a similar idea, implemented for the GEO 600 detector, is described in [23].

from the interferometric detector’s auxiliary channels. The consistency check is based on the observation of the coupling of different noise sources to the interferometer output strain channel. This veto was applied on LIGO S6 data [1, 2], and can be applied on data from Advanced LIGO and Advanced Virgo. In this paper we will fully describe the bilinear-coupling veto, and summarize its results when used on LIGO S6 data. We will also discuss its potential capabilities when used with data from Advanced LIGO and Advanced Virgo.

The organization of the paper is as follows. In Section II we describe the veto method. The results of the bilinear-coupling veto when applied to LIGO S6 data are given in Section III. In Section IV we discuss how the bilinear-coupling veto can be used as a potential diagnostic tool with the advanced detectors. Concluding observations are given in Section V.

II. INSTRUMENTAL VETO METHODS USING NOISE COUPLING MODELS

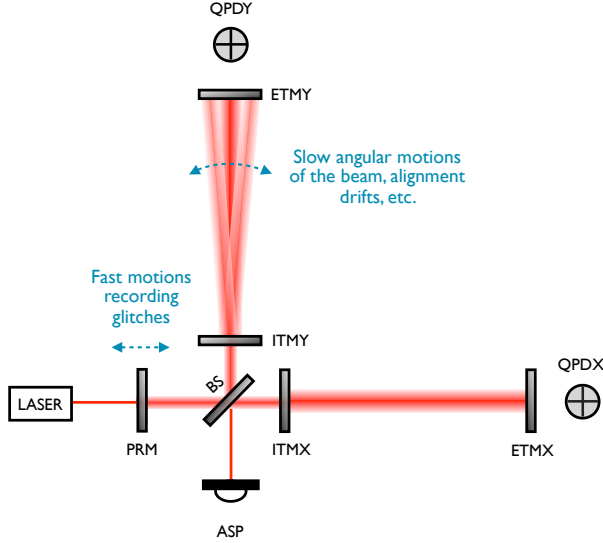


FIG. 1: Schematic diagram of a power recycled Michelson interferometer. Examples of motions recorded in “primary” and “secondary” channels are shown. The angular motion shown in the figure is greatly exaggerated. The beam need only move a few millimeters away from its optimal position on the mirror to create a non-optimal detector “state”. The label PRM stands for power recycling mirror, BS for beam splitter and ASP for antisymmetric (“dark”) port; see Section III for a description of other interferometer components.

“Traditional” veto methods that look for time-coincidence between triggers in the GW channel and an auxiliary channel have been quite successful in reducing the rate of spurious triggers in the GW channel. However, more powerful veto methods can be formulated making use of the information contained in the time-series data recorded in the two channels as well as our empirical understanding of the coupling of different noise sources to the GW channel. An instrumental veto method making use of the knowledge of the coupling of different detector subsystems to the GW channel was proposed in Refs. [24, 25]. The main idea behind this method was that the noise recorded

by an instrumental channel X can be *transferred* [26, 27] to the GW channel H provided the noise coupling is *linear* and the transfer function is known. This allows us to predict how a glitch witnessed by an auxiliary channel X would appear in the GW channel H . If a glitch is found in the GW channel at the same time and is consistent with the “prediction”, then it can be vetoed with high confidence. This method was found to be a very efficient veto method in the fifth science run of GEO 600 [24].

Here we present a powerful veto method using a more complex, *bilinear*-coupling model. The choice of the bilinear-coupling model is motivated by the empirical observations [28–30] from the LIGO interferometers that glitches witnessed by auxiliary channels appear in the GW channel only at particular epochs of time, suggesting a time-varying transfer function for the coupling of noise from the auxiliary channel to the GW channel. For example, glitches in the channel recording the signal controlling the length of the power-recycling cavity are found to couple to the GW channel only during particular states of the detector. Signatures of such instabilities are recorded in many other channels. For example, slow drifts in the alignment of mirrors can cause the position of the laser beam to wander around the mirror surfaces, which can potentially affect the coupling of the glitches in channel recording the Michelson control signal to the GW channel. Such slow, angular motions are recorded by the quadrant photodiodes (QPDs) placed behind the end-mirrors. This suggests that the signal recorded by the photodiode contains some information of the time-varying transfer function describing the coupling of the power-recycling control with the GW channel. A schematic diagram of the power-recycled Michelson interferometer is given in Figure 1.

In this paper, we denote the “primary channels” (channels recording fast motions such as glitches) by X_i and “secondary channels” (those recording slow configuration changes such as alignment drifts, slow angular motions of the beam, etc.) by Y_j . Table I lists some of the potential mechanisms in which a bilinear combination of “primary” and “secondary” channels couple to the GW channel.

We consider a simple model of the coupling between a combination of instrumental channels and the GW channel. In particular, our hypothesis is that many of the glitches in the GW channel H (with time series data $h(t)$) can be “best-witnessed” by a bilinear combination of a primary channel X_i and a secondary channel Y_j . i.e.,

$$h(t) \propto p_{ij}(t), \quad (2.1)$$

where

$$p_{ij}(t) \equiv x_i(t) y_j(t) \quad (2.2)$$

denote the data from a “pseudo channel” P_{ij} which is a bilinear combination of $x_i(t)$ and $y_j(t)$, the time-series data recorded in X_i and Y_j .

The consistency of the glitches in the GW channel H with the pseudo channel P_{ij} can be tested by computing the linear correlation coefficient between $p_{ij}(t)$ and $h(t)$, over an appropriate frequency band:

$$r_{ij} \equiv \frac{\langle h, p_{ij} \rangle}{\|h\| \|p_{ij}\|}, \quad (2.3)$$

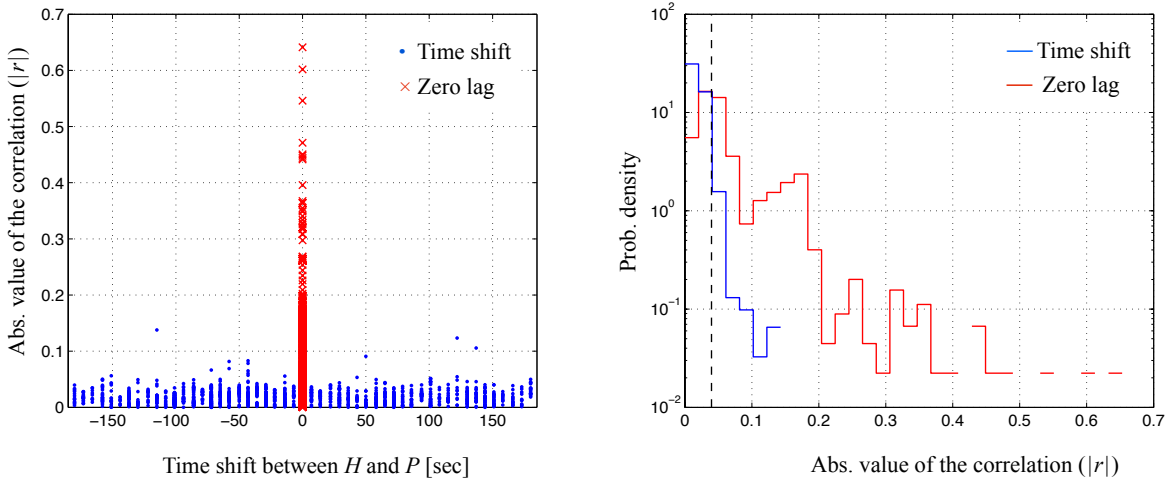


FIG. 2: An example of the correlation of a pseudo channel P_{ij} with the GW channel H . The left panel shows the absolute value of the linear correlation coefficient r between H and P_{ij} as a function of the time shift between the channels, while the right panel shows the distribution of $|r|$ from the time-shifted coincidences (blue) and zero lag (red). The pseudo channel is constructed from a bilinear combination of LSC-MICH_CTRL channel and ASC-QPDY_P from the L1 detector.

Primary channel (X_i)	Secondary channel (Y_i)
Length feedback control signals (e.g., LSC-MICH_CTRL, LSC-PRC_CTRL)	Beam position on the mirrors (e.g., ASC-QPD{X,Y}_{P,Y})
Angular torque feedback control signals (e.g., ASC-ETM{X,Y}_{P,Y})	Beam position on the mirrors (e.g., ASC-QPD{X,Y}_{P,Y})
Length feedback control signals (e.g., LSC-MICH_CTRL, LSC-PRC_CTRL)	Interferometer misalignment signals (e.g., ASC-WFS{1,2}_Q{P,Y})

TABLE I: Examples of potential bilinear-coupling mechanisms in LIGO detectors. Bilinear combinations of the primary and secondary channels, $x_i(t)y_i(t)$, have been found to be correlated to the GW channel. See Section III for a description of the channel names.

where the angular brackets denote inner products, and $\|a\| \equiv \langle a, a \rangle$ denotes the magnitude of the vector a . That is,

$$\langle a, b \rangle \equiv \int_{f_{\min}}^{f_{\max}} \tilde{a}(f) \tilde{b}^*(f) df, \quad (2.4)$$

where $\tilde{a}(f)$ is the Fourier transform of the time series data $a(t)$ over some time duration comparable to the duration of the glitch under consideration, and f_{\min} and f_{\max} are appropriately chosen low and high frequency cutoffs (e.g., from the bandwidth of the glitch under consideration, as estimated by a glitch detection algorithm)².

We compute the correlation coefficient r_{ij} between $p_{ij}(t)$ and $h(t)$ at the time of a coincident trigger in the primary instrumental channel X_i and the GW channel H . If the trigger in H is causally related to the one in X_i , and if our coupling model is realistic, we expect $|r_{ij}| \gg 0$. On the other hand, if the coincidence of the triggers in H and X is expected to be purely accidental, we expect $|r_{ij}| \sim 0$. An appropriately determined threshold λ_{ij} can be used to decide whether the correlation is significant. If $|r_{ij}| > \lambda_{ij}$, the trigger in H can be vetoed.

In order to determine an appropriate threshold, it is important to understand the “background” distribution of r_{ij} – the distribution of r_{ij} arising from purely accidental correlations. In order to estimate the background distribution of r_{ij} , we time shift the data between the auxiliary channels and the GW channel (by an amount much larger than the correlation length of the data), so that all the real correlations between the auxiliary channels and the GW channel are removed. Any remaining correlations between the channel pairs are purely accidental. We then identify coincident noise transients between the channel pairs and compute r_{ij} using data surrounding the triggers. An example of such “time-shift” analysis is shown in Figure 2, along with the correlations in the “zero lag” (no time shift applied between the channel pairs so that the correlations are real). A suitable threshold on r_{ij} can be found from the time-shifted analysis so that only an acceptable number of “background triggers” have r_{ij} greater than the threshold. This threshold can be used to decide which of the coincident triggers in the zero lag should be vetoed.

A schematic diagram of the vetoing algorithm is given in Figure 3. First we identify noise transients in the GW channel H and one “primary” instrumental channel X_i using an appropriate event trigger generator (such as KW). Coincident triggers between H and X_i are identified, allowing a time-window of the order of a second for coincidence. A pseudo channel P_{ij} is constructed according to Eq. (2.2) for a selected set of can-

² In the work reported in Sec. III, a fixed frequency range of 32–4096 Hz was chosen as the burst detection algorithm KW does not estimate the bandwidth of the glitch.

Primary channels X_i	Secondary channels Y_j
ASC-ETMX_{P,Y}	ASC-QPDX_{P,Y}
ASC-ETMY_{P,Y}	ASC-QPDY_{P,Y}
ASC-ITMX_{P,Y}	ASC-WFS1_Q{P,Y}
ASC-ITMY_{P,Y}	ASC-WFS2_I{P,Y}
LSC-MICH_CTRL	ASC-WFS2_Q{P,Y}
LSC-PRC_CTRL	ASC-WFS3_I{P,Y}
	ASC-WFS4_I{P,Y}

TABLE II: Auxiliary channels used for the bilinear-coupling veto analysis in the S6 data. Pseudo channels were constructed using all the 140 bilinear combinations $x_i(t)y_j(t)$. See the text for a description of various channels.

didates for Y_j . The linear correlation coefficient r_{ij} between H and P_{ij} is computed at the time of each coincident trigger in zero lag and in each time shift. The distribution of r_{ij} from the time-shifted analysis gives the background distribution of the correlation. A threshold λ_{ij} is chosen such that only a very small fraction of the coincident triggers in the time shift have r_{ij} greater than the threshold. After that, the analysis is repeated without applying any time shift between H and X_i (“zero-lag” analysis), and all coincident triggers with $r_{ij} > \lambda_{ij}$ are vetoed.

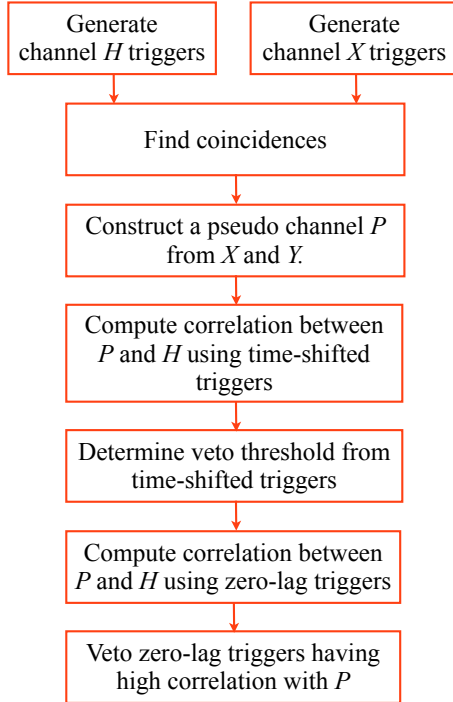


FIG. 3: Schematic diagram of the veto analysis pipeline.

III. APPLICATION TO DATA FROM THE SIXTH SCIENCE RUN OF LIGO

The sixth science run (S6) of the LIGO-Livingston (L1) and LIGO-Hanford (H1) detectors lasted from 7 July 2009 to 20 October 2010, and 141 days of coincident H1-L1 science quality data was collected during this run. Owing to a number

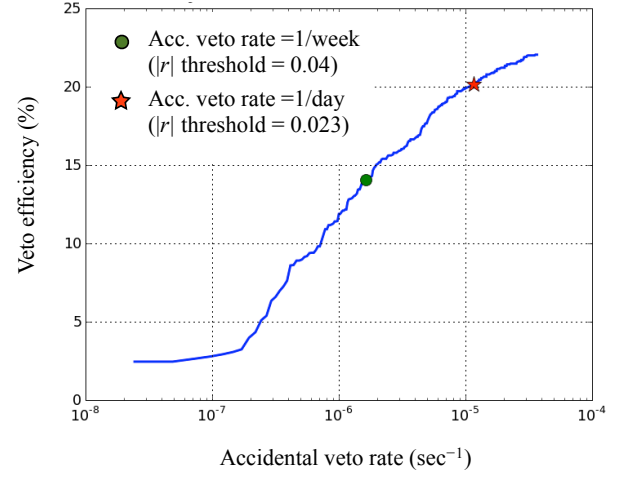


FIG. 4: The veto efficiency (fraction of triggers in H vetoed in the zero lag) as a function of the accidental veto rate (fraction of triggers in H vetoed per unit time in the time shifted analysis). The pseudo channel for this example is constructed from a bilinear combination of LSC-MICH_CTRL channel and ASC-QPDY_P from the L1 detector. The veto efficiency and accidental veto rate are computed by changing the veto thresholds. The green circle and the red star correspond to accidental veto rates of 1 per week and 1 per day, respectively. Thresholds corresponding to an accidental veto rate of 1 per week were used for the final veto analysis.

of improvements made on the LIGO detectors, the sensitivity of the detectors was in general better than the previous science runs. However, the rate of non-Gaussian noise transients was found to be larger than in the previous science runs. A number of instrumental veto techniques, as noted in Section I, were employed to reduce many of the noise transients in the data to be analyzed, and hence to improve the sensitivity of the searches for transient GW signals. Here we summarize the veto analysis performed on the S6 data using the bilinear-coupling veto pipeline.

The detector [31] auxiliary channels which we found to be most useful for the bilinear veto analysis described in this paper are listed in Table II. We chose a set of 10 primary (fast) and 14 secondary (slow) auxiliary channels. In addition, we also perform the veto analysis using 10 primary channels assuming a linear coupling model. These channels are all from the LIGO interferometer sensing and control (ISC) system. No physical environment monitoring (PEM) channels were used for this bilinear veto analysis. The ISC channels are all derived from optical sensing of length degrees of freedom (LSC) or angular degrees of freedom (ASC) of the interferometer; the optical sensors are read out by (near-DC or radio frequency, RF) photodiodes, analog electronics, and analog-to-digital conversion at 16384 Hz for the LSC signals and 2048 Hz for the ASC channels. A digital control system is employed to maintain these degrees of freedom at their nominal values throughout the observational run. The most useful length sensing (LSC) channels, derived from readout of RF photodiodes sensing the laser beam reflected from the interferometer [32], were the one used to keep the power recycling cavity (PRC) resonant (LSC-PRC_CTRL), and the one used to keep the short Michelson (MICH) length fixed (LSC-MICH_CTRL). The most useful fast

angular sensing (ASC) channels, for both pitch (P) and yaw (Y) angular degrees of freedom, were the ones monitoring the LIGO arm cavity mirrors, which we refer to as test masses: the input test mass (ITM) and end test mass (ETM) on each of the X and Y arms. So, for example, ASC-ETMY_Y represents the (optically-based) signal monitoring the yaw angular degree of freedom of the end test mass on the interferometer’s Y arm. The most useful slow ASC channels were those from quadrant (near-DC) photodiodes monitoring the light transmitted through the ETMs on both arms (e.g., ASC-QPDX_P is the signal monitoring the pitch angular degree of freedom of the laser beam exiting the end of the X arm), and the quadrant RF photodiodes (wavefront sensors, WFS) monitoring light from the output ports of the interferometer to measure deviations from optimal global alignment in six angular degrees of freedom [33]. So, for example, ASC-WFS1_QP represents the wavefront sensor signal monitoring the pitch angular degree of freedom of the end test masses of the two interferometer arms (differentially).

From the primary and secondary auxiliary channels listed in Table II, 140 pseudo channels were constructed as bilinear combinations [see Eq.(2.2)]. In addition, we also performed veto analysis using a linear coupling model using the 10 primary auxiliary channels (where, we threshold on the correlation between the GW channel and the primary instrumental channels X_i). Transients in the primary auxiliary channels as well as the GW channel were detected using KW [18]. We considered KW triggers with signal-to-noise ratio (SNR) greater than 8. Coincidence triggers between the primary auxiliary and GW channels were identified using a time window of 0.5 seconds, and the veto analysis was performed using each of the 140 pseudo channels (using the bilinear-coupling model), and 10 primary channels (using the linear coupling model). Correlation coefficients for each set of coincident triggers were calculated as described in Section II. The length of the data used to compute the correlation coefficient was chosen to be the cumulative duration (typically less than a second) of the coincident triggers in the two channels. Fifty time shifts in the interval $[-180s, 180s]$ were performed for each channel pair to estimate the background distribution of the correlation coefficients. Thresholds estimated from this time shift analysis were used to veto coincident triggers in the zero lag. For choosing the thresholds on the correlation, we define some useful figures of merit. One is the *efficiency* of the veto, which is defined as the fraction of triggers in the GW channel vetoed in the zero lag. The second is the *accidental veto rate*, which is the number of accidentally vetoed triggers in the GW channel per unit time (since they happen to be correlated with the pseudo channel purely by chance). We estimate the accidental veto rate by counting the fraction of triggers in H vetoed per unit time in the time shifted analysis. Figure 4 shows an example of the tuning used to determine the veto thresholds. The plot shows the *veto efficiency* and the *accidental veto rate* for different veto thresholds. As expected, higher thresholds result in lower veto efficiencies and lower accidental veto rates. In the final analysis we choose thresholds corresponding to accidental veto rate of 1 per week. Essentially this mean that, given the glitch rates in the GW channel and the auxiliary channel that we consider, our pipeline will veto a maximum of one trigger in the GW channel per week because it happens to have an accidental correlation

Parameter	Value
Total number of (pseudo) channels	140 bilinear + 10 linear
Accidental veto rate	1 / week / pseudo channel
Threshold on veto significance	5
Threshold on trigger SNR	8
Threshold on safety probability	0.999

TABLE III: Parameters for the bilinear-coupling veto analysis performed in the S6 data.

(that is greater than the chosen threshold) with the particular pseudo channel under consideration. In addition to this, we also impose a threshold on the *significance* of the veto, defined as the fraction of vetoed triggers in the zero lag divided by the fraction of vetoed triggers in the time-shift analysis. Only those pseudo channels for which significance is greater than 5 are used for vetoing triggers in the GW channel. Table III provides a summary of the parameters used in the analysis.

Another important concern is the *safety probability* of the veto, which is the probability of vetoing an actual GW signal. In order to estimate the safety probability, we perform the veto analysis on the triggers generated from GW-like “hardware injections” (GW signals artificially injected to the hardware of the detector). Our estimate of the safety probability is 1 – fraction of hardware injections vetoed. While this estimate is limited by the number and the nature of hardware injections performed, this gives us a reasonable estimate of the safety of the veto. (~ 3000 [2700] injections of compact binary coalescences and unmodelled burst signals were performed in H1 [L1] during S6, out of which ~ 2000 [1600] were detected by KW). For the S6 analysis, only those pseudo channels for which the safety probability is greater than 0.999 were used to veto triggers in the GW channel. However, we found that over the whole analysis from S6, none of the hardware injections were vetoed using any of the pseudo channels that we used.

Figure 5 shows the distribution of the SNR of the KW GW triggers before and after applying the veto, for a particular week during the S6 run in L1, while Fig. 6 provides a quick summary of the bilinear-coupling veto analysis results generated in the S6 run. Figure 6 shows the weekly glitch rate (defined as the number of KW triggers per week with $\text{SNR} > 8$), the veto efficiency (fraction of triggers in the GW channel vetoed using all the 140 pseudo channels + 10 linear coupling channels), the *dead time* (fractional duration of the data that has been vetoed) and the ratio of the veto efficiency and dead time (a typical figure of merit used to quantify the effectiveness of a veto method) over the entire S6 run in H1 and L1. In summary, the bilinear-coupling veto was found to be an efficient veto method with acceptable background rate, very low dead time and very high safety during the S6 analysis. Along with other veto methods [19–21], which also provided comparable veto efficiency, this veto was used to reduce the background rates of searches for transient GWs [1, 2].

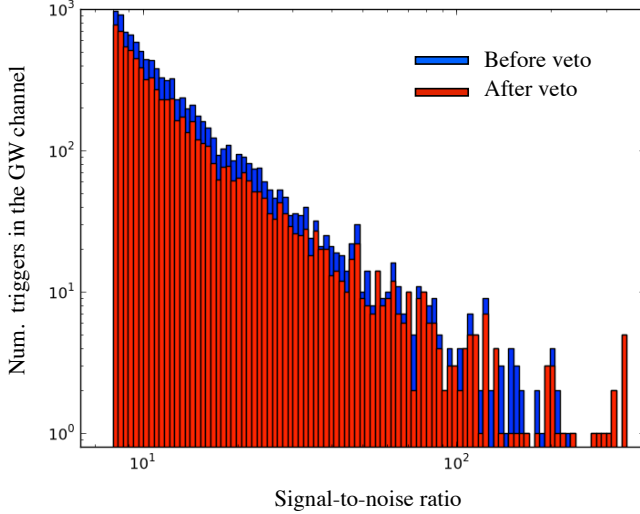


FIG. 5: The distribution of the signal-to-noise of the KW triggers in the GW channel before and after applying the bilinear-coupling veto. These triggers are from 1 week of L1 data starting from Oct 20 2009 01:12:42 UTC. Out of 9712 triggers in the GW channel, 2446 are vetoed.

IV. FUTURE WORK: BILINEAR VETO AS A POTENTIAL INTERFEROMETER DIAGNOSTIC TOOL

The idea of the bilinear veto is to see whether a pseudo instrumental channel is correlated with the GW channel at glitchy times. The pseudo channel P_{ij} is constructed as a bilinear combination of a “primary” instrumental channel X_i (which is producing glitches) and a “secondary” instrumental channel Y_j which acts as a coupling agent, or a time-varying transfer function. Often, the secondary channels come as orthogonal pairs (such as the pitch and yaw of the movement of a mirror). Thus, the pseudo channels P_{i1} and P_{i2} constructed from two orthogonal secondary channels Y_1 and Y_2 contain fairly independent information. We can combine the correlation coefficients (a complex number) of the two pseudo channels into a single value. That is, we define

$$r_i \equiv \sqrt{|r_{i1}|^2 + |r_{i2}|^2}, \quad (4.1)$$

where r_1, r_2 are the linear correlation coefficients of pseudo channels P_{i1} and P_{i2} with H . For certain channels, $(y_1(t), y_2(t))$ has a clear physical interpretation. For example, for the case of the secondary channels ASC-QPDX.P and ASC-QPDY.P this would correlate with the location of the beam spot on the two dimensional surface of the end-mirror of the Michelson cavity. If a significant fraction of the vetoed glitches are concentrated in a small region, that potentially suggest that the beam hitting on that particular position on the mirror makes it susceptible for the glitches in the the particular auxiliary channel to couple to the GW channel. This can be used as a potential diagnostic tool for the commissioners to identify non-optimal detector states.

This aspect of the bilinear-coupling veto analysis was not investigated in detail during the S6 analysis. However, preliminary investigations suggest this as a promising diagnostic tool. An example is shown in Figure 7, which plots the

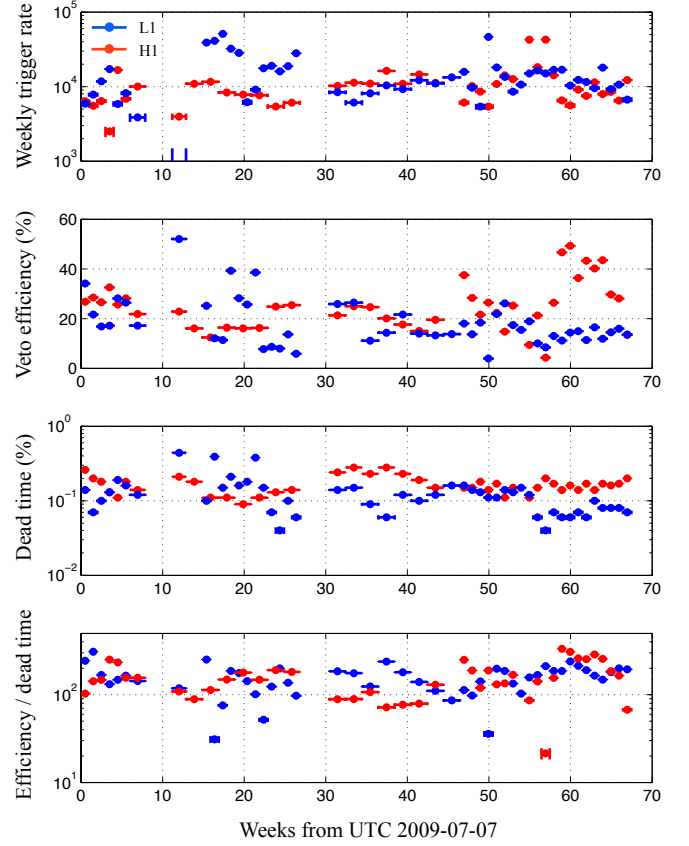


FIG. 6: A brief summary of the bilinear-coupling veto analysis performed on the S6 data in H1 and L1. The top panel shows the number of KW triggers from the GW channel per week, the second panel shows the veto efficiency (percentage of triggers vetoed), the third panel shows the dead time (percentage of observational data vetoed) and the bottom panel shows the ratio of the veto efficiency and dead time (a typical figure of merit used to quantify the effectiveness of a veto method).

measured values of an orthogonal pair of secondary channels (ASC-WFS2.L.P and ASC-WFS2.L.Y) at the times of coincident triggers between the GW channel and the control signal to the Michelson cavity (from one day of data on 15 Nov 2009). It can be seen that all the vetoed triggers (i.e., triggers in the GW channel that are highly correlated with the triggers in the pseudo channel under consideration) are clustered in a small region in the x-y plane. We plan to develop diagnostic tools based on more realistic bilinear-coupling models for the characterization of advanced GW detectors.

V. CONCLUSIONS

In this paper we have presented a description of a novel veto method that was recently used to eliminate short duration noise transients (glitches) in data from the LIGO detectors during the S6 science run [1, 2]. The unique aspect of the bilinear-coupling veto, as opposed to other vetoes used by LIGO and Virgo [19, 20, 22], is that it provides a means to identify and eliminate glitches in a detector’s output GW channel that are associated with non-optimal states of interferometer sub-systems; these

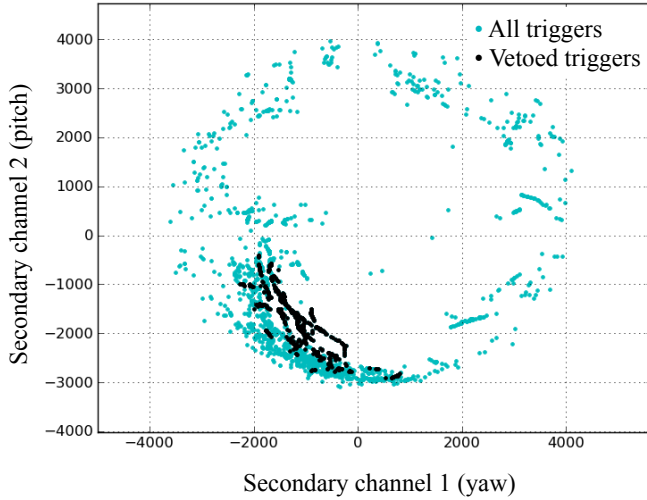


FIG. 7: The green dots correspond to the signal amplitude of the two secondary channels ASC-WFS2.I.P (pitch) and ASC-WFS2.I.Y (yaw) at the time of coincident glitches between L1-LSC-MICH_CTRL and H , and the black dots correspond to the vetoed triggers among them. This plot suggests that glitches in L1-LSC-MICH_CTRL couple to H only during times when ASC-WFS2.I.Pitch, Yaw are in certain “states”.

non-optimal states are observed in slow auxiliary channels, like the ones studied in this paper. This veto was also developed with the goal to see if the data from an interferometric detector’s output GW strain channel at the time of an apparent signal is consistent with the data from a detector auxiliary channel, or a combination of auxiliary channels. Results were presented demonstrating the effectiveness of this veto with LIGO S6 data.

For the case of the upcoming advanced detectors like Advanced LIGO [10] and Advanced Virgo [11, 12], the severity of noise glitches in the GW strain channels is presently unknown. If such glitches are found to limit the ability to detect GW

transient events, the the bilinear-coupling veto can be implemented as a means to reduce the number of noise transients. It should be noted, however, that Advanced LIGO and Advanced Virgo will reach their target sensitivities over a number of years of commissioning [13]. During this period it will be of critical importance to have tools that allow for the identification and characterization of noise. As demonstrated in this paper, the bilinear-coupling veto can be used as a means to diagnose sources of noise.

Another avenue for the improvement of the bilinear-coupling veto will be through the use of improved glitch trigger generators. The KW [18] pipeline will continue to be used to generate triggers. However, new trigger pipelines with improved resolution at low frequencies are being developed. We also note that several other noise regression methods using linear/bilinear coupling models are being investigated within the LIGO-Virgo collaboration [34–36]. We expect the bilinear-coupling veto to be a powerful noise diagnostic tool and veto generator for the next generation of laser interferometric GW detectors.

Acknowledgments

We thank the LIGO Scientific Collaboration for allowing us to use the LIGO data used to conduct this study and Peter Shawhan for his comments on this manuscript. LIGO was constructed by the California Institute of Technology and Massachusetts Institute of Technology with funding from the National Science Foundation and operates under cooperative agreement PHY-0757058. PA’s research was supported by the NSF grants PHY-0653653 and PHY-0601459, NSF career grant PHY-0956189, David and Barbara Groce Fund at Caltech, a FastTrack fellowship and a Ramanujan Fellowship from the Department of Science and Technology, India and by the EADS Foundation through a chair position on “Mathematics of Complex Systems” at ICTS-TIFR. NC’s research is supported by NSF grant PHY-1204371. This manuscript has the LIGO document number LIGO-P1400023-v2.

-
- [1] J. Abadie et al. (LIGO Collaboration, Virgo Collaboration), Phys. Rev. D **85**, 082002 (2012).
 - [2] J. Aasi et al. (LIGO Collaboration, Virgo Collaboration), Phys. Rev. D **87**, 022002 (2013).
 - [3] J. Abadie et al. (LIGO Collaboration, Virgo Collaboration), Phys. Rev. D **85**, 122007 (2012).
 - [4] C. Ott et al., Physical Review Letters **106**, 161103 (2011).
 - [5] J. Aasi et al. (LIGO Collaboration, Virgo Collaboration) (2013), 1310.2384.
 - [6] J. Aasi et al. (LIGO Collaboration, Virgo Collaboration), Phys. Rev. D **87**, 042001 (2012).
 - [7] B. Abbott et al. (LIGO Collaboration, Virgo Collaboration), Nature **460**, 990 (2009).
 - [8] B. Abbott et al., Astrophys. J. **760**, 12 (2012).
 - [9] S. Adrian-Martinez et al., Journal of Cosmology and Astroparticle Physics **6**, 008 (2013).
 - [10] G. M. Harry (LIGO Collaboration, Virgo Collaboration), Classical and Quantum Gravity **27**, 084006 (2010).
 - [11] F. Acernese et al. (Virgo Collaboration) (2009), URL <https://tds.ego-gw.it/ql/?c=6589>.
 - [12] F. Acernese et al. (Virgo Collaboration) (2012), URL <https://tds.ego-gw.it/ql/?c=8940>.
 - [13] J. Aasi et al. (LIGO Collaboration, Virgo Collaboration) (2013), 1304.0670.
 - [14] K. Somiya et al., Classical Quantum Gravity **29**, 124007 (2012).
 - [15] N. Christensen (LIGO Collaboration, Virgo Collaboration), Classical and Quantum Gravity **27**, 194010 (2010).
 - [16] J. Aasi et al. (LIGO Collaboration, Virgo Collaboration), Classical and Quantum Gravity **29**, 155002 (2012).
 - [17] M. Coughlin (LIGO Collaboration, Virgo Collaboration), J.Phys.Conf.Ser. **243**, 012010 (2010).
 - [18] S. Chatterji, L. Blackburn, G. Martin, and E. Katsavounidis, Classical and Quantum Gravity **21**, S1809 (2004).
 - [19] J. Smith et al., Classical and Quantum Gravity **28**, 235005 (2011).
 - [20] T. Isogai (LIGO Collaboration, Virgo Collaboration), J.Phys.Conf.Ser. **243**, 012005 (2010).
 - [21] D. MacLeod, S. Fairhurst, B. Hughey, A. Lundgren, L. Pekowsky, et al., Class.Quant.Grav. **29**, 055006 (2012), 1108.0312.
 - [22] T. Ballinger (LIGO Collaboration, Virgo Collaboration), Classi-

- cal and Quantum Gravity **26**, 204003 (2009).
- [23] M. Hewitson and P. Ajith, *Class.Quant.Grav.* **22**, 4903 (2005).
 - [24] P. Ajith et al., *Phys. Rev. D* **76**, 042004 (2007), 0705.1111.
 - [25] P. Ajith, M. Hewitson, J. Smith, and K. Strain, *Class.Quant.Grav.* **23**, 5825 (2006), gr-qc/0605079.
 - [26] R. Adhikari, Ph.D. thesis, Massachusetts Institute of Technology (2004).
 - [27] J. Smith, P. Ajith, H. Grote, M. Hewitson, S. Hild, H. Lück, K. Strain, B. Willke, J. Hough, and K. Danzmann, *Classical and Quantum Gravity* **23**, 527 (2006).
 - [28] S. Whitcomb, “*Bi-linear*” *noise mechanisms in interferometers* (2000), presentation at GWDAAW, LIGO-G000336-00-D, URL <https://dcc.ligo.org/LIGO-G000336/public>.
 - [29] D. Shoemaker, private communication.
 - [30] R. Weiss, private communication.
 - [31] B. Abbott et al. (LIGO Scientific Collaboration), *Rept.Prog.Phys.* **72**, 076901 (2009), 0711.3041.
 - [32] P. Fritschel, R. Bork, G. González, N. Mavalvala, D. Ouimette, H. Rong, D. Sigg, and M. Zucker, *Appl. Opt.* **40**, 4988 (2001).
 - [33] P. Fritschel, N. Mavalvala, D. Shoemaker, D. Sigg, M. Zucker, and G. González, *Appl. Opt.* **37**, 6734 (1998).
 - [34] V. Tiwari et al., *Regression of linear and bi-linear noise in LIGO* (2012), LIGO Internal Document, LIGO-G1200288-v1.
 - [35] S. Klimenko, *Regression of LIGO/Virgo data* (2012), LIGO Internal Document, LIGO-G1200197-v1.
 - [36] M. Drago, *Regression of LIGO/Virgo data* (2012), LIGO Internal Document, LIGO-G1200278-v6.